New insights into electron transport due to azimuthal drift in a Hall effect thruster

Kentaro Hara, Yusuke Yamashita, Sedina Tsikata, Benjamin Vincent, Stéphane Mazouffre, Shinatora Cho

New insights into electron transport due to azimuthal drift in a Hall effect thruster

IEPC-2019-691

Presented at the 36th International Electric Propulsion Conference
University of Vienna, Austria
September 15-20, 2019

Kentaro Hara*,
Stanford University, Stanford, California, 94305, USA
Texas A&M University, College Station, Texas, 77845, USA

Yusuke Yamashita,
University of Tokyo, Hongo, Tokyo, Japan

Sedina Tsikata, Benjamin Vincent, and Stéphane Mazouffre,
ICARE, CNRS UPR 3021, 1C ave de la Recherche Scientifique, 45071 Orléans, France

and

Shinatora Cho
Japan Aerospace Exploration Agency, Chofu, Tokyo, Japan

Partially magnetized plasmas in the Hall effect thrusters remain poorly understood primarily due to the electron transport in the cross-field direction. It is recently discussed that the drift-diffusion approximation is invalid for the electron dynamics in the presence of a large drift velocity. It is therefore possible that the anomalous electron transport is strongly related with the presence of an azimuthal drift. In this paper, we discuss the importance of the azimuthal drift on cross-field electron transport based on some recent results from a one-dimensional particle-in-cell simulation, two-dimensional particle-in-cell simulation, and laser Thomson scattering measurements.

I. Introduction

With the increasing demand and interest from the community, Hall effect thrusters (HETs) are one of the key space propulsion technologies.[1] The electric propulsion (EP) community has collected a wide range of knowledge and has expanded the capabilities of the thrusters to a level where these devices are used for various missions for scientific, military, and commercial purposes. While the focus of the HET research has been focused on designing new thrusters, establishing testing facilities, and developing experimental diagnostic capabilities, the community still lacks of predictive modeling capabilities that are critical in growing the industry and proposing new technologies based on the understanding gained through the computational and theoretical models.

Many computational models have been developed to simulate the discharge plasmas and plume of the HETs. The three main computational methods[2] that are developed so far are (i) a fluid approach, (ii) a particle-based kinetic approach, and (iii) a grid-based kinetic approach. In addition, fluid approaches include various formulations based on the assumptions. While the kinetic methods are useful for studying the

*Assistant Professor, Aeronautics and Astronautics, kenhara@stanford.edu

instabilities and non-Maxwellian nature of the plasmas, the computational challenges in the HET plasma, in particular in the channel, come from the multiscale nature of the problem. For instance, the spatial gradient of the plasma parameters, such as the plasma density and electron temperature, results in a variation of characteristic temporal and spatial scales. The plasma density can vary one to three orders of magnitude and the electron temperature may vary from a few electron-volts to a few tens of electron-volts. Hence, a fluid approach is still popularly used in the HET community due to the cheaper computational cost required. For instance, the computational cells do not have to resolve the characteristic spatial lengths, such as the Debye length, when a quasineutral assumption is used. This is attracting especially when one needs to model a large domain, e.g. anode-to-cathode including the plume to evaluate the thruster properties.

A fluid model, in general, refers to a computational and theoretical framework where macroscopic quantities, such as the density, bulk velocity, and temperature, are solved using conversation laws. Furthermore, for electrons, the community has utilized the drift-diffusion approximation, or the generalized Ohm's law, to simplify the computation. The effective collision mobility across the magnetic field lines is often assessed using the plasma measurements, such as the ion density, electron temperature, and electrostatic potential. Such experimental data are fed into the drift-diffusion flux formulation. The discrepancy between the observed effective electron mobility from the classical theory which only accounts for the collisional momentum transfer mechanisms is then often alluded to as the *anomalous electron transport*. Recent experimental observations and theoretical studies have suggested that the azimuthal plasma waves induced by instabilities, such as the electron cyclotron drift instability (ECDI),[3–5] are responsible for the electron detrapping from the magnetic field lines, namely, cross-field electron transport.

While the HET community adopted the drift-diffusion flux due to the wide use in the low-temperature plasma community, the most significant difference between conventional low-temperature, low-pressure plasma discharges and the HET discharge, i.e. partially magnetized ions is the azimuthal drift. Hence, in this paper, we attempt to analyze the effects of the azimuthal drift on the cross-field electron transport.

II. Derivation of the fluid equations

The Boltzmann equation can be written as

$$\frac{\partial f}{\partial t} + \vec{v} \cdot \frac{\partial f}{\partial \vec{x}} + \frac{q}{m}\left(\vec{E} + \vec{v} \times \vec{B}\right) \cdot \frac{\partial f}{\partial \vec{v}} = \frac{\delta f}{\delta t}, \tag{1}$$

where f is the velocity distribution function (VDF), which is a function of space $\vec{x}$, velocity $\vec{v}$, and time t, q is the elementary charge, $\vec{E}$ is the electric field, $\vec{B}$ is the magnetic field, and the right hand side is the collision term. The fluid equations, i.e. conservation laws, can be derived by taking the moments of the kinetic equation.

A. Cartesian coordinate

Let us assume that the magnetic field is only in one direction, e.g. z, for simplicity. The zeroth moment of the Boltzmann equation gives the continuity equation:

$$\frac{\partial n}{\partial t} + \frac{\partial}{\partial x}\left(n u_x\right) + \frac{\partial}{\partial y}\left(n u_y\right) = \dot{n}, \tag{2}$$

where $n = \int f dv^3$ is the number density, $u_i = \int v_i \hat{f} dv^3$ is the bulk velocity in the $i = x, y$ direction, $\hat{f} = f/n$ is the normalized VDF, and $\dot{n}$ is the source and sink terms due to volumetric reactions.

Taking the first moment of the Boltzmann equation, see Eq. (1), the momentum equations can be derived. Here, the collisional drag terms are assumed to follow the Krook's operator. The x-momentum equation can be written as,

$$\frac{\partial}{\partial t}(n u_x) + \frac{\partial}{\partial x}\left(n \int v_x^2 \hat{f} dv^3\right) + \frac{\partial}{\partial y}\left(n \int v_x v_y \hat{f} dv^3\right) = \frac{q}{m} n (E_x + u_y B_z) - (\nu_m + \nu_{\text{ion}}) n u_x, \tag{3}$$

and the y-momentum equation:

$$\frac{\partial}{\partial t}(n u_y) + \frac{\partial}{\partial x}\left(n \int v_x v_y \hat{f} dv^3\right) + \frac{\partial}{\partial y}\left(n \int v_y^2 \hat{f} dv^3\right) = \frac{q}{m} n (E_y - u_x B_z) - (\nu_m + \nu_{\text{ion}}) n u_y, \tag{4}$$

where ν_m is the momentum transfer collision frequency and ν_{ion} is the ionization frequency. The Lorentz force term is derived using integration by parts. In the conservative form of the momentum equation, the momentum loss due to the ionization means that the secondary electron generated results in an overall decrease of momenta. The inertia term is kept as the second moment of the VDfs.

B. Special condition of Cartesian coordinate system: when the flow is collisional

Here we discuss how the fluid equations, e.g. Navier Stokes, are derived. If the flow is collisional and the VDF is a Maxwellian distribution based on the local macroscopic quantities at any given time and location,

$$\hat{f} = \left(\frac{m}{2\pi k_B T_x}\right)^{1/2} \left(\frac{m}{2\pi k_B T_y}\right)^{1/2} \exp\left[-\frac{m(v_x-u_x)^2}{2k_B T_x}\right] \exp\left[-\frac{m(v_y-u_y)^2}{2k_B T_y}\right], \tag{5}$$

where T_x and T_y are the temperature in x and y directions, respectively and k_B is the Boltzmann constant. Thus, the second moments of the VDFs can be calculated as

$$\int v_x^2 \hat{f} dv^3 = n_0 u_x^2 + p_{xx}, \tag{6}$$

$$\int v_x v_y \hat{f} dv^3 = n_0 u_x u_y, \tag{7}$$

$$\int v_y^2 \hat{f} dv^3 = n_0 u_y^2 + p_{yy}, \tag{8}$$

where p_{xx} and p_{yy} are the pressure terms. Only then the fluid formulations, e.g. computational fluid dynamics, can be obtained.

$$\frac{\partial}{\partial t}(nu_x) + \frac{\partial}{\partial x}(nu_x^2) + \frac{\partial}{\partial y}(nu_x u_y) = -\frac{1}{m}\frac{\partial p_{xx}}{\partial x} + \frac{q}{m} n(E_x + u_y B_z) - (\nu_m + \nu_{\text{ion}}) n u_x, \tag{9}$$

$$\frac{\partial}{\partial t}(nu_y) + \frac{\partial}{\partial x}(nu_x u_y) + \frac{\partial}{\partial y}\left(nu_y^2\right) = -\frac{1}{m}\frac{\partial p_{yy}}{\partial y} + \frac{q}{m} n(E_y - u_x B_z) - (\nu_m + \nu_{\text{ion}}) n u_y. \tag{10}$$

C. Cylindrical coordinate

For a cylindrical coordinate system, assuming azimuthal symmetry (e.g. $\partial/\partial\theta = 0$), the Boltzmann equation can be written as

$$\frac{\partial f}{\partial t} + v_r \frac{\partial f}{\partial r} + v_z \frac{\partial f}{\partial z} + \left(a_r - \frac{v_\theta^2}{r}\right)\frac{\partial f}{\partial v_r} + \left(a_\theta + \frac{v_\theta v_r}{r}\right)\frac{\partial f}{\partial v_\theta} + a_z \frac{\partial f}{\partial v_z} = \frac{\delta f}{\delta t}, \tag{11}$$

where a_r, a_θ, and a_z are the acceleration terms in the r, θ, and z directions, respectively. Namely, $\vec{a} = q/m(\vec{E} + \vec{v} \times \vec{B}$. The difference between the Cartesian coordinate system is that the centrifugal forces contribute to the derivations.

Using integration by parts, the velocity advection terms introduce new terms. For instance, for the continuity equation, $\int (v_\theta v_r/r)\partial_\theta f dv^3 = (1/r)\int v_r f dv^3$, which can be lumped into the $\partial/\partial r$ term. The continuity equation can be written as

$$\frac{\partial n}{\partial t} + \frac{1}{r}\frac{\partial}{\partial r}(rnu_r) + \frac{\partial}{\partial z}(nu_z) = \dot{n}. \tag{12}$$

The $r-$, $\theta-$, and $z-$momentum equations are given as

$$\frac{\partial}{\partial t}(nu_r) + \frac{1}{r}\frac{\partial}{\partial r}\left(r\int v_r^2 f dv^3\right) + \frac{\partial}{\partial z}\left(\int v_r v_z f dv^3\right) = \frac{q}{m} n(E_r + u_\theta B_z) - (\nu_m + \nu_{\text{ion}}) n u_r + \int \frac{v_\theta^2}{r} f dv^3, \tag{13}$$

$$\frac{\partial}{\partial t}(nu_\theta) + \frac{1}{r}\frac{\partial}{\partial r}\left(r\int v_r v_\theta f dv^3\right) + \frac{\partial}{\partial z}\left(\int v_\theta v_z f dv^3\right) = \frac{q}{m} n(E_\theta + u_z B_r - u_r B_z) - (\nu_m + \nu_{\text{ion}}) n u_\theta - \int \frac{v_\theta v_r}{r} f dv^3, \tag{14}$$

$$\frac{\partial}{\partial t}(nu_z) + \frac{1}{r}\frac{\partial}{\partial r}\left(r\int v_r v_z f dv^3\right) + \frac{\partial}{\partial z}\left(\int v_z^2 f dv^3\right) = \frac{q}{m} n(E_z - u_\theta B_r) - (\nu_m + \nu_{\text{ion}}) n u_z. \tag{15}$$

Note that the second moments are not denoted using any fluid quantities yet, since they can strictly speaking only be written using fluid quantities when the VDFs are Maxwellian (see the previous section).

III. Evidence of electron azimtuhal velocity

Incoherent Thomson Scattering (ITS) measurements on two 200 W Hall thrusters, both magnetically shielded and non-shielded thrusters, are conducted. Both thrusters are equipped with $BNSiO_2$ channels and have the same channel width and mean diameter. This technique has been used to measure the plasma properties in the hollow cathode plume.[6] The scattered light is collected as a function of frequency, which gets translated into the electron velocity. Hence, the VDF of the electrons can be measured.

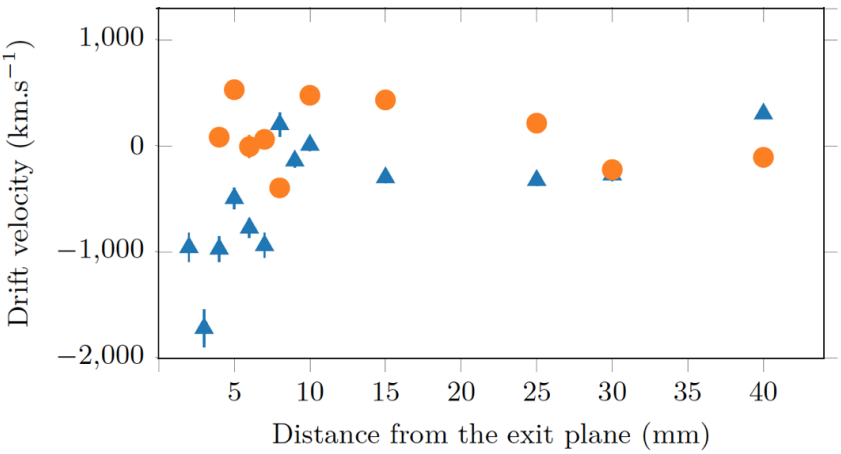

Figure 1: The drift velocity along both azimuthal and radial directions, obtained from laser Thomson scattering. Reproduced from 7.

Figure 1 shows the recent result from Vincent et al. in which the azimuthal drift can be observed much larger than the radial drift obtained from the Gaussian distribution of the sampled signals. This is the first unambiguous signal of the azimuthal velocity. The maximum magnetic field strength is 150 G and the discharge voltage is 250 V. The measured current is 1.14 A. As can be seen from Fig. 1, the maximum azimuthal drift detected is approximately 2×10^6 m/s, which corresponds to a kinetic energy of 11 eV. Note that the radial drift velocity is on the order of a few hundred kilometers per second, which corresponds to less than 1 eV.

IV. 1D Analysis

A particle-in-cell (PIC) simulation is developed to model the discharge characteristics in the axial direction.[8] Before attempting to build a self-consistent model, we use an artificial anomalous electron transport profile which generates a steady-state discharge current trace without any breathing mode oscillations. This way, the numerical analysis becomes straightforward without the need to account for the effects of the low-frequency oscillations.

The computational domain is similar to geometry of a SPT-100 type thruster. The channel length is 2.5 cm and the near-field plume is accounted for by extending the domain 2.5 cm. Hence, the domain size if 5 cm. The outer and inner radii are 5 mm and 3.45 mm, respectively. The mass flow rate is 5 mg/s and the propellant is xenon. The full-PIC simulation utilizes the electron mass of 9.1×10^{-31} kg and permittivity of 8.85×10^{12} F/m. The number of cells is 2500 to resolve the Debye length. An explicit PIC simulation is used where the equations of motion are solved for individual computational macroparticles. The collisions are accounted for using the Monte Carlo Collision method. In the calculation, we utilize the quasineutral injection method from the cathode, which injects the electrons to satisfy local quasineutrality at the last computational cell. The ions and electrons are absorbed on the anode. The radial channel wall is not accounted for in the results shown here. Particle decomposition is used to accelerate the simulation using message passing interface (MPI). Since the simulation solves for the 1D field properties, the Poisson solver is performed in a single core after gathering the ion and electron densities. Note that the results shown here exhibit negative azimuthal velocity due to the orientation of magnetic field, namely, the simulation corresponds to a case where the magnetic field is pointing inward.

The anomalous mobility is taken into consideration to achieve steady-state results. Here, a two-region model is adopted, where the anomalous momentum transfer collision frequency is $\nu_{\text{ano}} = \omega_{ce}/160$ inside the channel and $\nu_{\text{ano}} = \omega_{ce}/16$ outside the channel, where $\omega_{ce} = eB/m$ is the electron gyrofrequency.[9] The ECDI suggests that the momentum transfer of electrons is solely in the perpendicular direction so the parallel dynamics is unaffected. This corresponds to perpendicular scattering where the axial and azimuthal velocities are exchanged. However, other instabilities, such as modified two-stream instability, allow for momentum exchange in the parallel direction. Thus, we also investigate the effects when isotropic scattering is used for the anomalous components. Momentum transfer due to electron-neutral collisions is modeled accounting for the elastic collision, excitation, and ionization. For the results shown, an isotropic scattering is assumed for momentum transfer via all electron-neutral collisions.

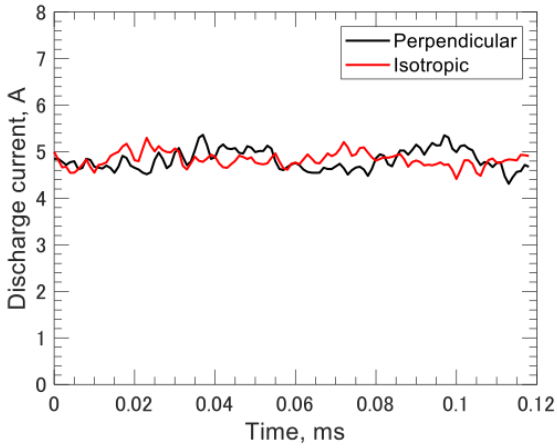

Figure 2: The discharge current trace using a 1D PIC simulation assuming perpendicular and isotropic scattering for the anomalous mobility treatment.

Figure 2 shows the discharge current, namely, the anode current, when the artificial anomalous transport is considered to be perpendicular and isotropic scattering. For perpendicular scattering, $v_\perp$ and v_y are exchanged, while isotropic scattering assumes momentum exchange in all directions, i.e. $v_\perp$, v_y, and v. Both results show good agreement for the time-averaged current around 4.8 A. This illustrates that the results are insensitive to the parallel dynamics via the anomalous scattering.

Figure 3 shows the instantaneous plasma properties obtained from the 1D PIC simulation. The PIC results agree qualitatively with the quasineutral fluid solver except near the boundaries. The plasma sheaths form near the anode. The sheath potential of which is a few electron temperature, which is smaller than the sheath potential required for a floating potential, meaning that the electrons are conducted through the anode. The axial electron bulk velocity near the anode reaches about -5×10^5 m/s. Additionally an acceleration of azimuthal bulk velocity can be observed near the anode, which is due to the kinetic effects where the gyrating electrons are absorbed. The azimuthal velocity is approximately -1.7×10^6 m/s at maximum and then plateaus in the near field plume where a large anomalous "artificial" momentum transfer mechanism is accounted for. From the emission plane, stationary electrons are assumed for the injected components. Thus, a decrease of the azimuthal bulk velocity can be seen near the injection plane.

Now, the effects of the inertia terms, including the azimuthal drift components, on electron transport can be evaluated. Neglecting the variation in y, a steady-state solution of Eqs. 3 and 4 can be given by

$$\overline{nu_x} = -\mu_0(\overline{nE_x} + \overline{nu_y}B_z) - \frac{1}{\nu_m}\overline{\frac{\partial}{\partial x}\left(\int v_x^2 f dv^3\right)}, \tag{16}$$

$$\overline{nu_y} = -\mu_0(\overline{nE_x} - \overline{nu_x}B_z) - \frac{1}{\nu_m}\overline{\frac{\partial}{\partial x}\left(\int v_x v_y f dv^3\right)}, \tag{17}$$

where $\mu_0 = e/(m\nu_m)$ is the nonmagnetized electron mobility. The importance of Eq. 16 is that the cross-field transport is dependent on the inertia term (which we will see that this can be reduced to a known form) and the azimuthal drift. If the drift-diffusion approximation holds, u_y is simply Ωu_x, which gives the classical diffusion.

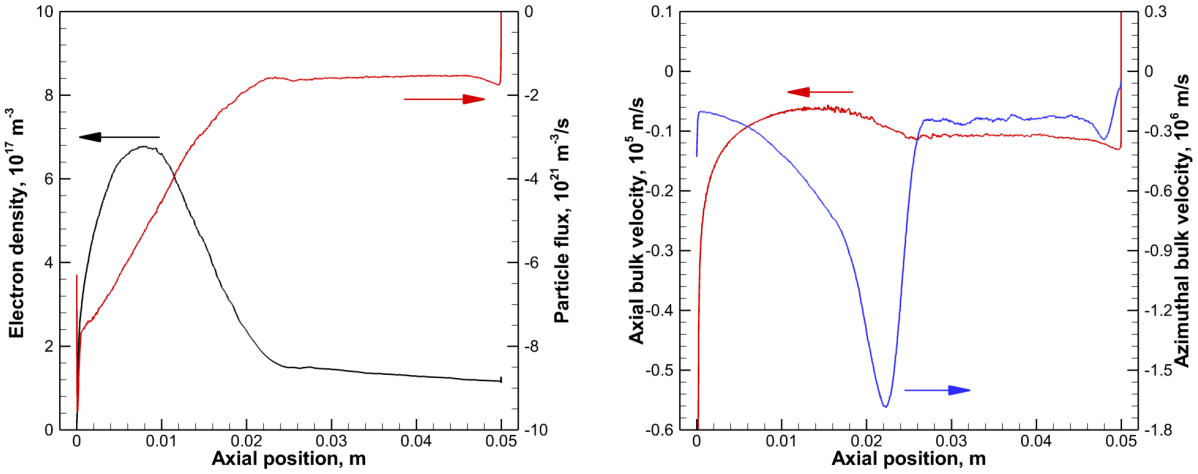

Figure 3: Instantaneous results. Left: electron density and electron axial flux density. Right: electron axial and azimuthal bulk velocities.

If one considers $f = f_0 + f'$, where f_0 is the equilibrium Maxwellian VDF and f' is the perturbed VDF, the inertia terms discussed in Eqs. 16 and 17 can be written as,

$$\int v_x^2 (f_0 + f') dv^3 = n u_x^2 + p_{xx} + R_{xx}, \tag{18}$$

$$\int v_x v_y (f_0 + f') dv^3 = n u_x u_y + p_{xy} + R_{xy}, \tag{19}$$

where $R_{xx} = \int v_x^2 f' dv^3$ and $R_{xy} = \int v_x v_y f' dv^3$.

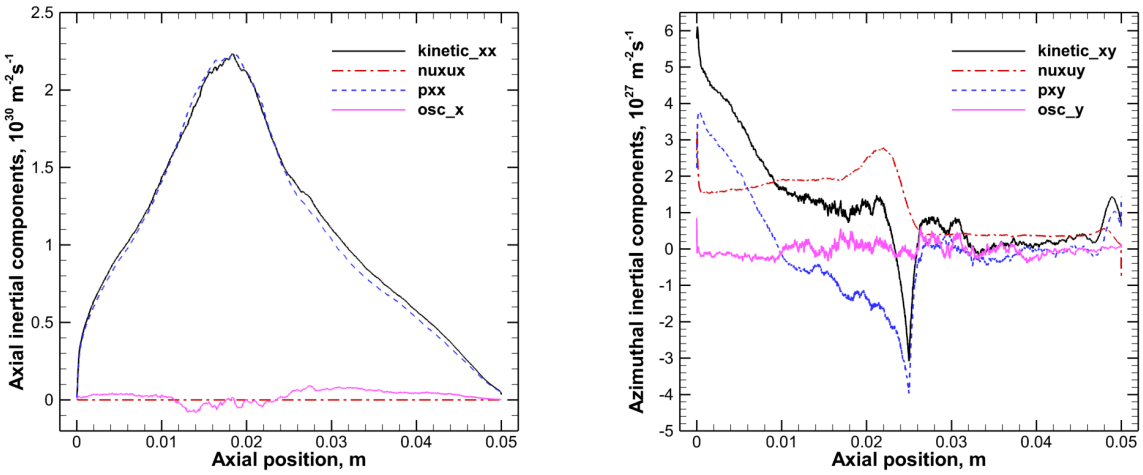

Figure 4: The inertia flux density. Left: xx contributions. Right: xy contributions. Denoted as *kinetic_xx* and *kinetic_xy* are the second moment of the VDFs and other terms correspond to the right hand side of Eqs. 18 and 19.

Figure 4 shows the contribution of each macroscopic terms. It can be seen that the PIC results show the second moment for $v_x v_x$ is dominantly the pressure term. Thus, the x-momentum equation can be simplified

to

$$\overline{nu_x} = -\mu_0 \left(\overline{nE_x} + \frac{1}{e} \frac{\partial \overline{p_{xx}}}{\partial x} + \overline{nu_y} B_z \right), \tag{20}$$

which is equivalent to the drift-diffusion formula. However, the second moment of $v_x v_y$ exhibits a more complex structure. If drift-diffusion approximation were to hold, the nu_y flux equation (from the y-momentum equation) will follow a similar form as Eq. (22). It can be seen from Fig. 4(left) that the oscillatory component, i.e. R_{xy} in Eq. 19, is almost negligible. However, due to the presence of a large u_y, $\int v_x v_y f dv^3$ is not equal to p_{xy} alone nor $nu_x u_y$ alone. Thus,

$$\overline{nu_y} = -\mu_0 \left(\frac{1}{e} \frac{\partial \overline{nu_x u_y} + \overline{p_{xy}}}{\partial x} - \overline{nu_x} B_z \right). \tag{21}$$

By combining Eqs. 22 and 21, the axial cross-field flux density can be written as

$$\overline{nu_x} = -\frac{\mu_0}{(1+\Omega^2)} \left[\left(\overline{nE_x} + \frac{1}{e} \frac{\partial \overline{p_{xx}}}{\partial x} \right) + \Omega \left(\frac{1}{e} \frac{\partial \overline{nu_x u_y} + \overline{p_{xy}}}{\partial x} \right) \right], \tag{22}$$

V. 2D analysis

A 2D cylindrical full PIC simulation is used to model the HET discharge plasmas.[10,11] Singly, doubly, and triply charged ions are included. No artificial electron mass nor permittivity is used. More details of the simulations will be discussed in IEPC-2019-718.

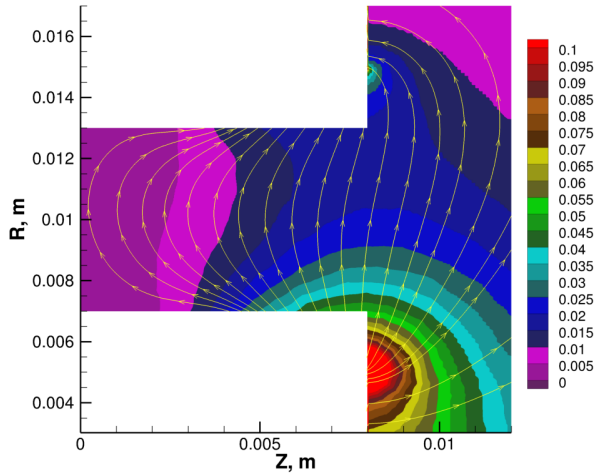

Figure 5: Magnetic field strength (unit: Tesla) and lines in a HET.

The magnetic field strength and lines are shown in Fig. 5. There is a path in the cross-field direction that the minimal magnetic field strengths can be achieved, which is possibly the lowest conductivity path for the electrons. However, it can be seen that the vectors of the magnetic field are curved in a HET configuration. In the presence of boundary conditions at the wall (inside the channel and pole pieces), anode, and electron injection, the plasma behaves in a complex fashion.

Figure 6 shows the regions where the azimuthal bulk velocity is positive and the corresponding electron density. From Eqs. 13, 14, and 15, the steady-state momentum equations can be written as

$$\overline{\frac{1}{r}\frac{\partial}{\partial r}\left(r \int v_r^2 f dv^3 \right)} + \overline{\frac{\partial}{\partial z}\left(\int v_r v_z f dv^3 \right)} = \frac{q}{m}(\overline{nE_r} + \overline{nu_\theta} B_z) - \nu_m \overline{nu_r} + \overline{\int \frac{v_\theta^2}{r} f dv^3}, \tag{23}$$

$$\overline{\frac{1}{r}\frac{\partial}{\partial r}\left(r \int v_r v_\theta f dv^3 \right)} + \overline{\frac{\partial}{\partial z}\left(\int v_\theta v_z f dv^3 \right)} = \frac{q}{m}(\overline{nE_\theta} + \overline{nu_z} B_r - \overline{nu_r} B_z) - \nu_m \overline{nu_\theta} - \overline{\int \frac{v_\theta v_r}{r} f dv^3}, \tag{24}$$

$$\overline{\frac{1}{r}\frac{\partial}{\partial r}\left(r\int v_r v_z f dv^3\right)} + \overline{\frac{\partial}{\partial z}\left(\int v_z^2 f dv^3\right)} = \frac{q}{m}(\overline{nE_z} - \overline{u_\theta} B_r) - \nu_m \overline{n u_z}. \tag{25}$$

For simplicity, let us derive the drift-diffusion like equation by neglecting the inertia terms on the left hand side in Eqs. 23, 24, and 25.

$$0 = -\frac{e}{m}\left(E_r + \frac{1}{en}\frac{\partial p_{rr}}{\partial r}\right) - \nu_m u_r + \frac{u_\theta^2}{r}, \tag{26}$$

$$0 = -\frac{e}{m}\left(u_z B_r\right) - \nu_m u_\theta - \frac{u_\theta u_r}{r}, \tag{27}$$

$$0 = -\frac{e}{m}\left(E_z + \frac{1}{en}\frac{\partial p_{zz}}{\partial z} - u_\theta B_r\right) - \nu_m u_z. \tag{28}$$

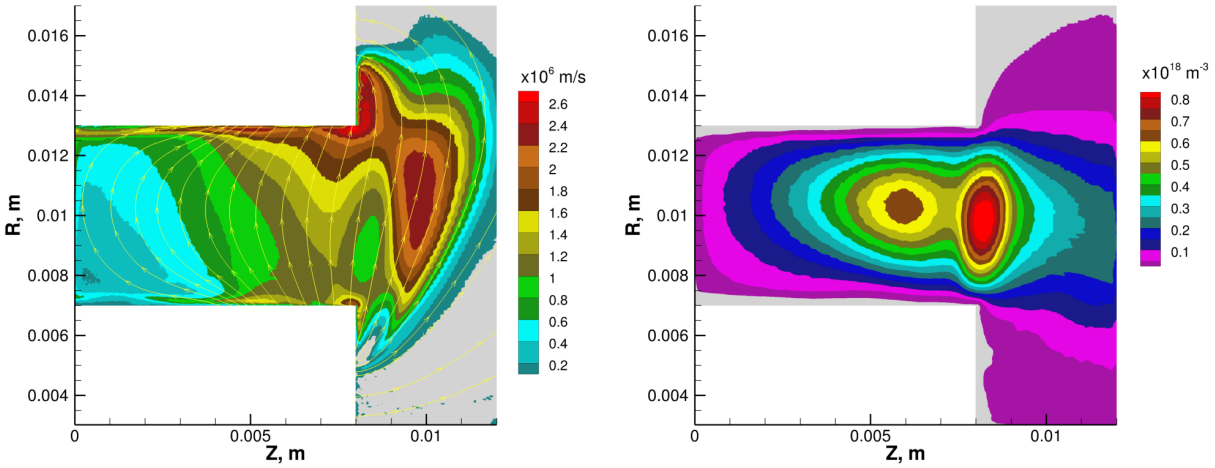

Figure 6: The azimuthal bulk velocity (left) and the electron density (right). The negative azimuthal bulk velocities are turned off to clearly show the positive velocity regions. In addition, the plasma density that is below 0.1% of the maximum electron density (8×10^{17} m^{-3}) is turned off.

From Eq. 27,

$$u_\theta = -\frac{\omega_B u_z}{\nu_m + \frac{u_r}{r}} = -\frac{\Omega}{1 + \frac{u_r}{r\nu_m}} u_z, \tag{29}$$

where $\omega_B = eB/m$ is the gyrofrequency. Inserting Eq. 30 into Eq. 28 gives

$$\left(1 + \frac{\Omega^2}{1 + \frac{u_r}{r\nu_m}}\right) u_z = -\mu_0 \left(E_z + \frac{1}{en}\frac{\partial p_{zz}}{\partial z}\right). \tag{30}$$

This indicates that the radial bulk velocity may contribute to the cross-field electron transport as well.

VI. Conclusion

This paper reports the derivations of the fluid equations taking the moments from the kinetic equations. First, the importance of the inertia terms is explained. It can be observed that from a full 1D PIC simulation, the axial inertia term reduces to the pressure term while the azimuthal inertia term is a combination of the shear and pressure terms, which could cause the anomalous electron transport.

In addition, the results from the full 2D PIC simulation are used to discuss the importance of the azimuthal drift through the centrifugal force term. The presence of centrifugal force plays an important role in the azimuthal momentum equation, which shows that the cross-field electron transport can be affected by the radial electron transport parallel to the magnetic field lines.

VII. Acknowledgments

This material is based upon work supported by the Air Force Office of Scientific Research under award number FA9550-18-1-0090 and work supported by the US Department of Energy, Office of Science, Office of Fusion Energy Sciences under Award Number DE-SC0019045.

References

[1]Boeuf J P 2017 *J. Appl. Phys.* **121** 011101
[2]Hara K 2019 *Plasma Sources Sci. Technol* **28** 044001
[3]Tsikata S and Minea T 2015 *Phys. Rev. Lett.* **114** 185001
[4]Janhunen S, Smolyakov A, Chapurin O, Sydorenko D, Kaganovich I and Raitses Y 2018 *Phys. Plasmas* **25** 011608
[5]Boeuf J P and Garrigues L 2018 *Phys. Plasmas* **25** 061204
[6]Vincent B, Tsikata S, Mazouffre S, Minea T and Fils J 2018 Plasma Sources Sci. Technol. **27** 055002
[7]Vincent B, Tsikata S and Mazouffre S (submitted)
[8]Yamashita Y, Hara K, Cho S and Nishiyama K (in preparation)
[9]Hara K 2018 *Phys. Plasmas* **25** 123508
[10]Cho S, Komurasaki K and Arakawa Y 2013 *Phys. Plasmas* **20** 063501
[11]Cho S, Watanabe H, Kubota K, Iihara S, Fuchigami K, Uematsu K and Funaki I 2015 *Phys. Plasmas* **22** 103523